Revision of the Theory of Tracer Transport and the Convolution Model of Dynamic Contrast Enhanced Magnetic Resonance Imaging

Stephen L. Keeling[1], Roland Bammer[2] and Rudolf Stollberger[3]

Abstract. Counterexamples are used to motivate the revision of the established theory of tracer transport. Then dynamic contrast enhanced magnetic resonance imaging in particular is conceptualized in terms of a fully distributed convection-diffusion model from which a widely used convolution model is derived using, alternatively, compartmental discretizations or semigroup theory. On this basis, applications and limitations of the convolution model are identified. For instance, it is proved that perfusion and tissue exchange states cannot be identified on the basis of a single convolution equation alone. Yet under certain assumptions, particularly that flux is purely convective at the boundary of a tissue region, physiological parameters such as mean transit time, effective volume fraction, and volumetric flow rate per unit tissue volume can be deduced from the kernel.

Keywords: convection, diffusion, perfusion, permeation, tracer, transport, DCE-MRI, convolution, nonidentifiability.

Running Title: Revision of the Theory of Tracer Transport and the Convolution Model of DCE-MRI.

1 Introduction

A major goal in functional magnetic resonance imaging is to evaluate tissue perfusion, or fluid flow, and the exchange between tissues and blood, or vessel permeability. For instance, ischemic tissues are characterized by a low oxygen state due to inadequate blood flow. On the other hand, tumors are characterized by excessive vascularization and a corresponding increase in blood flow. Further, the transport mechanisms involved may be convection or diffusion dominated when the volumetric flow rate is large or small, respectively, in relation to vessel permeability for instance. To evaluate the transport states of tissues, a bolus of contrast agent is injected into a patient, and rapid magnetic resonance imaging techniques are used to follow the concentration time course of the contrast agent at a given tissue site. The present paper grew out of the authors' efforts to develop estimation techniques by which dynamic contrast enhanced magnetic resonance imaging (DCE-MRI) data may be used to quantify the transport states described here [13]. While attempting to clarify precisely what can be determined from these data, it was discovered that the theory of tracer transport and the convolution model of DCE-MRI requires revision. The purpose of this paper is to explain the need for revision and to present a new foundation for the theory. In a follow-up paper [14], the authors present their nonparametric deconvolution techniques whose applicability is naturally constrained by the theoretical results reported here.

[1]Institut für Mathematik und Wissenschaftliches Rechnen, Karl-Franzens-Universität Graz, Heinrichstraße 36, 8010 Graz, Austria; email: stephen.keeling@uni-graz.at; tel: +43–316–380–5156; fax: +43–316–380–9815. Supported by the Fonds zur Förderung der wissenschaftlichen Forschung under SFB 03, "Optimierung und Kontrolle".

[2]Radiological Sciences Laboratory, R. Lucas MRS/I Center, Department of Radiology, Stanford University, 1201 Welch Road, Stanford, CA 94305-5488, USA; email: rbammer@stanford.edu; tel: +1–650–498–4760; fax: +1–650–723–5795. Supported by a grant from the National Institutes of Health (NIH-R01-EB002711).

[3]Abteilung für Klinische und Experimentelle Magnetresonanzforschung, Universitätsklinik für Radiologie, Medizinische Universität Graz, Auenbruggerplatz 9, 8036 Graz, Austria; e-mail: rudolf.stollberger@meduni-graz.at; tel: +43–316–385–3529; fax: +43–316–385–3848. Supported by the Fonds zur Förderung der wissenschaftlichen Forschung under SFB 03, "Optimierung und Kontrolle".

In Section 2 simple examples are used to motivate the need for revision of the mathematical formulation of tracer transport given in the foundational work of [26] and cited in most recent works, e.g., [10], [11], [15], [18], [23]. Specifically, by means of explicit solutions it is shown in Section 2 that while the physiological mechanisms of interest in [26] are represented in Fig. 1b, the mathematical formulation appearing in that work applies to Fig. 1a.

A new theoretical foundation for tracer transport and DCE-MR imaging is presented in Section 3 in terms of a fully distributed convection-diffusion model; note the emphasis on distributed parameter modeling of capillary-tissue exchange in [16] and see also further semi-distributed models in [7] and the references cited therein. A well known convolution model is newly derived from the present convection-diffusion model using, alternatively, compartmental discretizations or semigroup theory. In the convolution form of the model, an arterial input concentration of contrast agent is convolved with a desired convolution kernel, which is the impulse response of a given tissue region. With the convection-diffusion formulation, the limits of applicability of the convolution formulation are conveniently illuminated. Specifically, detailed results established in Appendices A and B are used to characterize the tissue states described above and to identify them as spectrally distinct. Further, it is shown that the convolution model requires concentration flux at a tissue boundary to be purely convective. Under this and other stated conditions, the physiological parameters which have received the most attention in the literature and which can be computed from the convolution kernel are derived anew. These include the volumetric flow rate per unit tissue volume, the mean transit time, and the effective volume fraction; see, e.g., [19].

Examples are also given in [5], and the references cited therein, in which the kernel shape must be determined accurately. Further, the kernel shape has been fit to parametrized compartment models [15] [23], particularly in an effort to identify the tissue states described above [10], [11], [18]. However, it is shown in the present work that these tissue states cannot be decided on the basis of a single convolution equation alone. Specifically, it is proved here that a given transport kernel can be approximated arbitrarily well by one for a tissue in which transport is purely convective. Nevertheless, in the follow-up work [14], nonparametric regularized deconvolution methods for kernel estimation are presented which permit the determination of the kernel shape and physiological parameters which can be deduced from it.

2 The Motivating Examples

The aim of this section is to motivate the need for revision of the mathematical formulation of tracer transport given in the foundational work of [26] and cited in most recent works, e.g., [10], [11], [15], [18], [23]. The point can be made clearly by considering the simple compartmental models shown in Fig. 1, which are chosen for ease of explanation while related distributed

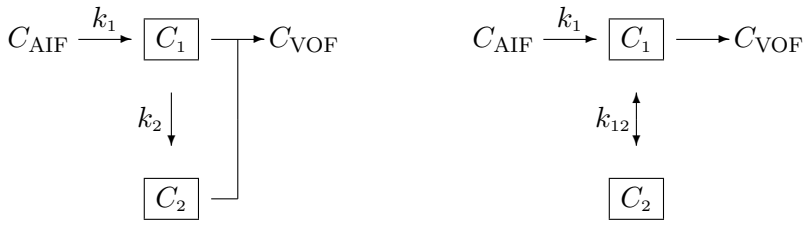

Figure 1: Compartment networks with (a) purely convective exchange shown on the left, and (b) convective and diffusive exchange shown on the right. The parameters in (3.2) may be chosen so that the respective residue functions are identical.

parameter formulations discussed later would make the point perhaps more realistically. The typical notation of the established theory is used here and briefly explained but then intro-

duced systematically in Section 3. In both the examples of Fig. 1, a tissue region is divided into two compartments which are assumed to be well mixed and with constant volumes V_i. According to the usual assumptions, transport of a tracer into and out of the tissue region occurs only through concentration functions C_{AIF} and C_{VOF}, respectively, i.e., an arterial input function and a venous output function. Tracer concentration in compartment i is denoted by C_i. The passive transport mechanisms of convection and diffusion are represented respectively by unidirectional and bidirectional transport paths between compartments. The differential formulations of transport for Figs. 1a and 1b are given respectively by the following particular cases of (3.2):

$$\begin{array}{rcl} V_1C_1' + k_1(C_1 - C_{\mathrm{AIF}}) &=& 0 \\ V_2C_2' + k_2(C_2 - C_1) &=& 0 \end{array} \tag{2.1}$$

and:

$$\begin{array}{rcl} V_1C_1' + k_1(C_1 - C_{\mathrm{AIF}}) &=& k_{12}(C_2 - C_1) \\ V_2C_2' &=& k_{12}(C_1 - C_2). \end{array} \tag{2.2}$$

When the first and second compartments are regarded respectively as intravascular and extravascular spaces, Fig. 1b is clearly the more fitting description of perfusion and permeation in the tissue region. Specifically, perfusion is unidirectional convection, being driven by a fixed pressure gradient, while permeation is bidirectional diffusion being driven by a varying concentration gradient. Thus, a permeable substance injected into either the intra- or extravascular space would diffuse into the opposite space where the concentration is lower. Such bidirectional transport is not permitted in Fig. 1a. While the physiological mechanisms of interest in [26] are represented in Fig. 1b, the mathematical formulation used in the foundational work, as well as in others building on this foundation, applies to Fig. 1a. In order to justify this claim, the respective mathematical formulations must be given explicitly.

According to [26], if h_1 and h_2 are the distributions of tracer transit times through the intravascular and extravascular spaces respectively, and E is the fraction of tracer extracted from the intravascular space, then the distribution of tracer transit times through the tissue region is given by:

$$h(t) = (1 - E)h_1(t) + Eh_2(t) * h_1(t) \tag{2.3}$$

where $*$ denotes convolution. As shown below in relation to (3.25), the distribution of transit times for a given tissue region is the venous output function for that region resulting from an impulsive arterial input function. It will be shown by solving (2.2) that the diffusive connection between compartments 1 and 2 in Fig. 1b creates such a strong coupling between them that independent impulse responses cannot even be defined for these two compartments. However, impulse responses are readily defined for the compartments of Fig. 1a, and the solution to (2.1) agrees with (2.3) as will now be demonstrated.

Under the assumption that the initial tissue concentration is zero, the solution to (2.1) for an impulsive $C_{\mathrm{AIF}} = \delta$ is given by the following particular case of (3.4):

$$\begin{array}{rcl} C_1(t) &=& h_1(t) \\ C_2(t) &=& h_1(t) * h_2(t) \end{array} \quad \text{where} \quad h_i(t) = \mu_i e^{-\mu_i t}, \quad \mu_i = k_i/V_i. \tag{2.4}$$

The tracer concentration in the tissue region is given by the following particular case of (3.23):

$$C(t) = \frac{V_1C_1 + V_2C_2}{V_1 + V_2} = \frac{k_1}{V_1 + V_2}\left[e^{-\mu_1 t} + \frac{k_2}{V_1}e^{-\mu_1 t} * e^{-\mu_2 t}\right]. \tag{2.5}$$

As explained in relation to (3.24) and (3.25), the fraction of tracer remaining in the tissue after time t is $R(t) = C(t)/\lim_{s\to 0^+} C(s)$ and the distribution of transit times through the tissue region, or equivalently the impulse response of the tissue region, is given finally by:

$$h(t) = -R'(t) = (1 - E)h_1(t) + Eh_1(t) * h_2(t), \quad E = k_2/k_1. \tag{2.6}$$

Here, h_1 and h_2 can be identified as the impulse responses of compartments 1 and 2 in Fig. 1a as they are solutions to $V_i C_i' + k_i(C_i - \delta) = 0$. Also, since k_1 and k_2 are purely convective rate constants, E is the fraction of the flow into compartment 1 which is extracted into compartment 2 while the flow fraction $(1-E)$ continues toward the venous output. Clearly, (2.6) agrees with (2.3), and it will now be shown that the solution to (2.2) does not.

Under the assumption that the initial tissue concentration is zero, the solution to (2.2) for an impulsive C_{AIF} is given by the following particular case of (3.4):

$$\begin{aligned} C_1(t) &= \frac{k_1}{V_1V_2(\lambda_2-\lambda_1)}\left[(k_{12}-\lambda_1V_2)e^{-\lambda_1 t}-(k_{12}-\lambda_2V_2)e^{-\lambda_2 t}\right] \\ C_2(t) &= \frac{k_1k_{12}}{V_1V_2(\lambda_2-\lambda_1)}\left(e^{-\lambda_1 t}-e^{-\lambda_2 t}\right) \end{aligned} \tag{2.7}$$

where:

$$\begin{aligned} \lambda_1 &= (\alpha+\beta)/(2V_1V_2), & \alpha &= k_{12}(V_1+V_2)+k_1V_2, \\ \lambda_2 &= (\alpha-\beta)/(2V_1V_2), & \beta^2 &= (k_1V_2+k_{12}(V_1+V_2))^2-4k_1k_{12}V_1V_2. \end{aligned} \tag{2.8}$$

As with (2.5), the tracer concentration in the tissue region is given by:

$$\begin{aligned} C(t) = \frac{V_1C_1+V_2C_2}{V_1+V_2} = \frac{k_1}{V_1V_2(V_1+V_2)(\lambda_2-\lambda_1)}\times \\ \left[(k_{12}(V_1+V_2)-\lambda_1V_1V_2)e^{-\lambda_1 t}-(k_{12}(V_1+V_2)-\lambda_2V_1V_2)e^{-\lambda_2 t}\right] \end{aligned} \tag{2.9}$$

As with (2.6), with $R(t) = C(t)/\lim_{s\to 0^+} C(s)$ the impulse response of the tissue region is given finally by:

$$h(t) = -R'(t) = \frac{\lambda_1(k_{12}(V_1+V_2)-\lambda_1V_1V_2)}{V_1V_2(\lambda_2-\lambda_1)}e^{-\lambda_1 t} - \frac{\lambda_2(k_{12}(V_1+V_2)-\lambda_2V_1V_2)}{V_1V_2(\lambda_2-\lambda_1)}e^{-\lambda_2 t}. \tag{2.10}$$

Notice the dependence of the eigenvalues $-\lambda_1$ and $-\lambda_2$ of the system matrix in (2.2) upon parameters of both compartments. Thus, the compartments of the system are so strongly coupled that separate compartmental impulse responses cannot even be defined. Nevertheless, an extraction fraction can still be defined as seen in the discussion of (A.3).

Notice that the intra- and extravascular spaces may be arbitrarily finely compartmentalized, even represented by distributed parameter models, and yet so long as the two are in passive diffusive contact with one another, impulse responses can no more easily be defined for the two spaces than they can for the simple two-compartment model analyzed above. More serious still is the fact that one cannot determine by measurement of the impulse response of a tissue region whether that region is characterized by a model such as Fig. 1a or Fig. 1b. To see this, note from (2.6) and (2.10) that in both cases h (and R) are a sum of two exponentials. Given those exponentials, it cannot be determined whether the system eigenvalues are given by (2.4) or (2.8). This last observation is a special case of a general non-identifiability result established below in Theorem 2.

3 A Revised Theory

Since it has been shown in the previous section that the theory of [26] and related works requires revision, a new distributed parameter basis is proposed in this section with particular interest in deriving the convolution model of DCE-MRI. The derivation of the convolution model from within this framework critically demonstrates assumptions upon which the convolution model is based, but further allows a characterization of qualitatively distinct convolution

kernels in terms of their spectral properties. Furthermore, this characterization is used below to show that the associated distinct transport states cannot in general be identified from a single convolution equation alone, since a convection dominated kernel can be found which is indistinguishable from a given kernel.

3.1 Distributed Parameter Setting

The importance of distributed parameter modeling of capillary-tissue exchange is emphasized in [16], but existing models are semi-distributed in the sense that a system of concentrations is defined for a single capillary with parallel subregions at whose boundaries permeation is driven by jump discontinuities in concentration; see [7] and the references cited therein. Here, DCE-MR imaging is conceptualized in terms of a fully distributed convection-diffusion model in which permeation is driven by concentration gradients. For this, let Ω be a given tissue region containing both intravascular and extravascular spaces. According to the usual treatment of the continuum hypothesis [4], distributed quantities are defined pointwise by the limit of stable averages within ever smaller volumes. Specifically, let $\boldsymbol{v}$ be a vector field such that $\boldsymbol{v}$ has the same orientation as convection when convection is present and $[I - \boldsymbol{v}\boldsymbol{v}^{\mathrm{T}}]$ has the same orientation as permeation when permeation is present. Assume further that $\boldsymbol{v}$ is supported only in regions of convection or permeation, where $\boldsymbol{v}^{\mathrm{T}}\boldsymbol{v} = 1$ holds, and otherwise $\boldsymbol{v} = 0$. Let F (length/time) denote the mean fluid velocity supported only on regions of convection, where the measure of this support depends upon the extent of vascularization in Ω. Then the spatiotemporal distribution of contrast agent concentration C (mass/volume) is modeled by:

$$\partial_t C + \nabla \cdot (F\boldsymbol{v}C) = \nabla \cdot (\mathcal{D}(\boldsymbol{v})\nabla C), \qquad \mathcal{D}(\boldsymbol{v}) = D\boldsymbol{v}\boldsymbol{v}^{\mathrm{T}} + P[I - \boldsymbol{v}\boldsymbol{v}^{\mathrm{T}}] \tag{3.1}$$

where $\mathcal{D}$ is a diffusivity tensor which includes a convection oriented diffusivity D (area/time) and a permeation oriented diffusivity P. While D is convection oriented in the lumen, D is permeation orthogonal in a membrane. Similarly, P is permeation oriented in a membrane and convection orthogonal in the lumen. Furthermore, in a membrane $P = \mathcal{P}\tau$ depends upon a distributed permeability $\mathcal{P}$ (diffusivity/depth) and a distributed membrane thickness τ. In the interstitial space, $\boldsymbol{v} = 0$ holds and P is the local isotropic diffusivity. Naturally, when membranes are disrupted, the convective space must be enlarged from the lumen to include the portion of interstitial space in which flow is present. The diffusivity tensor $\mathcal{D}(\boldsymbol{v})$ may of course be generalized, but the diffusion mechanisms shown in (3.1) are those which have received the most attention in the literature [7]. The (contrast agent) influx and outflux portions of the boundary $\partial\Omega$ are the subsets where $F\boldsymbol{n}^{\mathrm{T}}\boldsymbol{v}C < \boldsymbol{n}^{\mathrm{T}}\mathcal{D}(\boldsymbol{v})\nabla C$ and $F\boldsymbol{n}^{\mathrm{T}}\boldsymbol{v}C > \boldsymbol{n}^{\mathrm{T}}\mathcal{D}(\boldsymbol{v})\nabla C$ hold, respectively, where $\boldsymbol{n}$ is the outward directed unit normal vector. The (fluid) inflow and outflow boundaries are the arterial inflow $F\boldsymbol{n}^{\mathrm{T}}\boldsymbol{v} < 0$ and venous outflow boundaries $F\boldsymbol{n}^{\mathrm{T}}\boldsymbol{v} > 0$, respectively. As seen in Section 2, diffusive exchange between Ω and its surroundings must be assumed zero in order to define an impulse response for Ω, and under this assumption, the influx and outflux boundaries coincide with the inflow and outflow boundaries respectively.

The tissue states described in Section 1 may be related to the convection-diffusion model as follows on the basis of the detailed results shown in Appendix A. First assume that transport is convection dominated. When the tissue is ischemic, F is supported on a smaller subset of Ω, and a concentration wave entering Ω remains more coherent during transit and exits with a very narrowly distributed transit time. In case of high vascularization, F is more widely supported in Ω, and a concentration wave entering Ω manifests more dispersion during transit and exits with a widely distributed, yet finite, transit time. Now assume that transport is not convection dominated so that flux into and out of Ω may occur by diffusion in addition to convection. In such cases, the mixing resulting from diffusion leads not only to considerable dispersion of entering concentration waves but the contrast agent clears from Ω only after infinite time as a result of upstream diffusion.

One approach to identify these different tissue states, which will be considered in a separate work, is to identify the coefficients in (3.1) from spatiotemporally distributed concentration data, see [2] and [3]. Alternatively, (3.1) may be integrated, in a compartmental setting or in a distributed setting, in order to develop an input-output model of the tissue region Ω.

3.2 The Measurement Process for DCE-MRI

To develop such an input-output model, consider what can be measured or inferred from DCE-MRI data. The images shown in Fig. 2 were taken from a series of magnetic resonance images measured during the injection of a Gadolinium-DTPA based contrast agent, where the

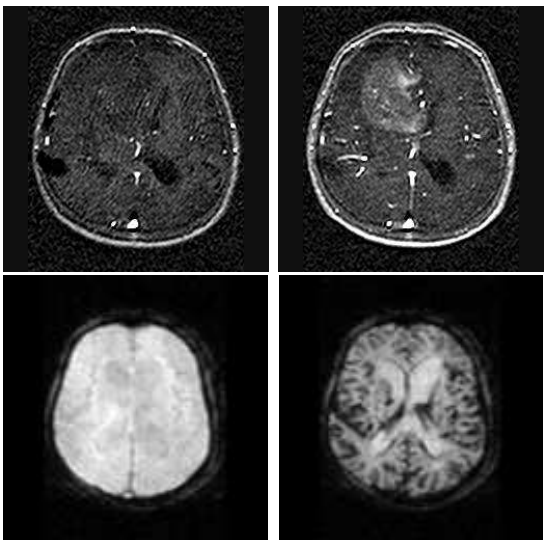

Figure 2: Magnetic resonance images taken from a series of images measured during the injection of a Gadolinium-DTPA based contrast agent. From left to right the images were taken, respectively, before and after the appearance of the contrast agent. The first row shows T_1-weighted images while the second row shows T_2^*-weighted images.

images shown from left to right were taken, respectively, before and after the appearance of the contrast agent. Note that the required temporal resolution causes a reduction in the signal-to-noise ratio. Note further in the T_1-weighted images that the contrast agent causes a local elevation in the otherwise rather uniform intensity while in the T_2^*-weighted images the contrast agent causes a local reduction in intensity. In both cases, the change in intensity improves image contrast, and the degree of intensity change can be quantitatively related to the local concentration of the contrast agent. Thus, once a tissue region Ω is identified, e.g., one pixel or a group of pixels, the contrast agent concentration in Ω can be determined from imaging. On the other hand, all contrast agent exiting Ω cannot be easily measured. Furthermore, the concentration of contrast agent entering Ω can only be approximated by the measured concentration in a nearby major artery.

3.3 Modeling Assumptions

Thus, in order to develop the desired input-output model of Ω, the following concentrations must be conceptually separated: the concentration C_{T} within the tissue Ω, an arterial input function C_{AIF}, and a venous output function C_{VOF}. However, it is evident from the solutions seen in Section 2, Appendix A and Appendix B that in order to avoid diffusive coupling between Ω and its surroundings and thereby isolate Ω for the desired model, *the concentration flux at the boundary of* Ω *must be assumed to be purely convective.* Further, it is assumed that *the fluid flow through every subset of* Ω *is balanced* so that $\int_{\partial D} F\boldsymbol{v}^{\mathrm{T}}\boldsymbol{n}d\boldsymbol{x} = 0$ holds for every $D \subseteq \Omega$. It is also

assumed that *the parameters F, $\boldsymbol{v}$, P, and D in (3.1) are time-independent*, and thus the tissue exhibits *stationarity* in the sense of [25]. Finally, it is assumed that *the concentrations C_{AIF} and C_{VOF} are spatially constant along the inflow and outflow boundaries respectively.* Although the authors are particularly interested in DCE-MRI applications as described in the previous subsection, the present analysis is intended to apply generally for all applications in which tracer is transported passively by convection and diffusion.

3.4 Compartmental Setting

Under these assumptions let Ω be divided into S subregions which are perfusion and permeation conforming, i.e., the subregion boundaries are either parallel or orthogonal to the vector field $\boldsymbol{v}$, and the boundary of the support of F is contained in the set of subregion boundaries. Let the subregions have respective concentrations $\{C_i\}_{i=1}^S$ which are numbered in such a way that in the support of F, convective transport proceeds from subregion $i-1$ to subregion i, so that (3.1) may be discretized as follows:

$$V_i C_i' + k_i(C_i - C_{i-1}) = \sum_{j \neq i} k_{ij}(C_j - C_i). \tag{3.2}$$

The volume of the ith subregion is V_i, and the non-negative coefficients k_i/V_i and k_{ij}/V_i may be interpreted as rate constants characterizing the kinetic exchange between compartments. Those compartments j for which $k_{ij} \neq 0$ holds are those having diffusive exchange with the ith compartment. While $k_{ij} = k_{ji}$ holds, the rate constants k_{ij}/V_i and k_{ji}/V_j are the same only when the respective compartments have identical volumes. In convective exchange with the upstream neighbor, the same convective constant k_i weights both C_i and $-C_{i-1}$ since the flow through a given compartment is assumed to be balanced. When the upstream convective reference is outside Ω, $k_i C_{i-1}$ refers to $k_i C_{\mathrm{AIF}}$. Note that subregions may exist outside the support of F which are inaccessible by passive transport so that $C_l = 0$ holds in such subregions; thus, the associated rate constants k_l/V_l and k_{lj}/V_l vanish. Since the arterial inflow concentration is assumed to be spatially constant, (3.2) can be written as:

$$V\boldsymbol{C}' = A\boldsymbol{C} + \boldsymbol{b}C_{\mathrm{AIF}} \tag{3.3}$$

where $\boldsymbol{C} = \langle C_1, \ldots, C_S \rangle^{\mathrm{T}}$, $V = \mathrm{diag}\{V_i\}_{i=1}^S$, $\boldsymbol{b} \in \boldsymbol{R}^S$ is the vector $\{k_i\chi_i : \chi_i = (C_{i-1} = C_{\mathrm{AIF}})\}$ and A is the matrix which represents all other multiplications shown in (3.2). Since the coefficients in (3.1) and thus (3.2) are assumed to be time-independent, the solution to (3.3) is given by:

$$\boldsymbol{C}(t) = \exp\left[V^{-1}At\right]\boldsymbol{C}(0) + \int_0^t \exp\left[V^{-1}A(t-s)\right]V^{-1}\boldsymbol{b}C_{\mathrm{AIF}}(s)ds. \tag{3.4}$$

The average tissue concentration is now given by $C_{\mathrm{T}} = \boldsymbol{e}^{\mathrm{T}}V\boldsymbol{C}/\boldsymbol{e}^{\mathrm{T}}V\boldsymbol{e}$, where here and below $\boldsymbol{e} \in \boldsymbol{R}^S$ denotes the vector $\boldsymbol{e} = \langle 1, 1, \ldots, 1 \rangle^{\mathrm{T}}$.

3.5 The Semigroup Formulation

The reader who prefers the compartmental analysis treatment of the previous subsection as the basis for the convolution model presented in the next subsection may wish to jump over this alternative treatment. Here, a counterpart to (3.4) is formulated with a semigroup in the distributed parameter setting; see [20] for further details.

The formulation of the associated Cauchy problem is motivated by the following formal modification of (3.1) which is now forced by the boundary input C_{AIF}:

$$\partial_t C + \nabla \cdot (F\boldsymbol{v}C) = \nabla \cdot (\mathcal{D}(\boldsymbol{v})\nabla C) + F\boldsymbol{v}^{\mathrm{T}}\boldsymbol{n}(C - C_{\mathrm{AIF}})\delta_{\partial\Omega}(F\boldsymbol{v}^{\mathrm{T}}\boldsymbol{n} < 0) \tag{3.5}$$

where the δ-function is concentrated on the inflow portion of $\partial\Omega$. The term on the right in (3.5) is chosen so that influx on $\Gamma = \{\partial\Omega : F\boldsymbol{v}^{\mathrm{T}}\boldsymbol{n} < 0\}$ is given by C_{AIF}, as demonstrated by integrating the last equation over Ω and applying the Gauss Theorem:

$$\int_\Omega \partial_t C d\boldsymbol{x} + \int_{\boldsymbol{v}^{\mathrm{T}}\boldsymbol{n}<0} F\boldsymbol{v}^{\mathrm{T}}\boldsymbol{n}C_{\mathrm{AIF}}d\boldsymbol{x} + \int_{\boldsymbol{v}^{\mathrm{T}}\boldsymbol{n}>0} F\boldsymbol{v}^{\mathrm{T}}\boldsymbol{n}Cd\boldsymbol{x} = \int_{\partial\Omega} \boldsymbol{n}^{\mathrm{T}}\mathcal{D}(\boldsymbol{v})\nabla C d\boldsymbol{x} = 0. \tag{3.6}$$

Since diffusive flux is assumed to be negligible on the boundary, the boundary condition $\boldsymbol{n}^{\mathrm{T}}\mathcal{D}(\boldsymbol{v})\nabla C = 0$ on $\partial\Omega$ causes the last term in (3.6) to vanish.

To avoid the technical matters associated with distributional solutions, let the δ-function in (3.5) be replaced by χ, the characteristic function vanishing outside a very narrow but smooth subset of Ω which borders on Γ with $\int_\Omega \chi d\boldsymbol{x} = 1$. Also define $\boldsymbol{n}$ on the support of χ by its value at the nearest point on Γ, and note from the definition of Γ that $\boldsymbol{v}^{\mathrm{T}}\boldsymbol{n} < 0$ holds on a sufficiently narrow support of χ. Then for an arbitrary $t^* > 0$, let the Cauchy problem be formulated as:

$$\left\{ \begin{array}{rcl} C' & = & \mathcal{A}C + \mathcal{B}C_{\mathrm{AIF}}, \quad 0 \le t \le t^* \\ C(0) & = & C_0 \end{array} \right. \tag{3.7}$$

where $\mathcal{A}$ and $\mathcal{B}$ are defined as follows. Here, $H^m(\Omega)$ is the usual Sobolev space of (measurable) functions whose (weak) derivatives up to order m are in $L_2(\Omega)$, and $H^m(\Omega)$ is equipped with the inner product $(\cdot,\cdot)_m$ and norm $\|\cdot\|_m$. Also $\mathcal{C}(U,V)$ denotes the space of continuous functions from U into V equipped with the sup-norm, and $L_\infty(\Omega)$ denotes space of essentially bounded (measurable) functions equipped with the essential sup-norm $\|\cdot\|_\infty$. See [17] for further details. Thus, the operator $\mathcal{A}$ and its domain $\mathrm{Dom}(\mathcal{A})$ are defined by:

$$\begin{array}{rcl} \mathcal{A}C & = & \nabla\cdot(\mathcal{D}(\boldsymbol{v})\nabla C) - \nabla\cdot(F\boldsymbol{v}C) + F\boldsymbol{v}^{\mathrm{T}}\boldsymbol{n}\chi C \\ \mathrm{Dom}(\mathcal{A}) & = & \{C \in H^2(\Omega) : \boldsymbol{n}^{\mathrm{T}}\mathcal{D}(\boldsymbol{v})\nabla C = 0, \partial\Omega\} \end{array} \tag{3.8}$$

and $\mathcal{B}$ is defined by:

$$\mathcal{B}C = -F\boldsymbol{v}^{\mathrm{T}}\boldsymbol{n}\chi C. \tag{3.9}$$

Now defining formally the semigroup $S(t) = \exp[\mathcal{A}t]$, the counterpart to (3.4) in the present distributed parameter setting is given by the following solution to the Cauchy problem (3.7):

$$C(t) = S(t)C_0 + \int_0^t S(t-s)\mathcal{B}C_{\mathrm{AIF}}(s)ds \tag{3.10}$$

as is proved in detail in Theorem 1 below. The average tissue concentration is then given from (3.10) by $C_{\mathrm{T}} = \int_\Omega C(t)d\boldsymbol{x}/\mathrm{vol}(\Omega)$.

For the proof of Theorem 1, uniform ellipticity of the differential operator is required:

$$\theta\|\boldsymbol{x}\|^2 \le \boldsymbol{x}^{\mathrm{T}}\mathcal{D}\boldsymbol{x}, \quad \forall \boldsymbol{x} \in \boldsymbol{R}^3. \tag{3.11}$$

Also, note that (3.7) is said to have a *weak* solution C for $C_{\mathrm{AIF}} \in L_2([0,t^*], L_2(\Omega))$ if $C \in \mathcal{C}([0,t^*], L_2(\Omega))$ and:

$$\begin{array}{c} \displaystyle\int_0^{t^*} (X, C)_0 dt + \int_0^{t^*} (Y, \mathcal{B}C_{\mathrm{AIF}})_0 dt + (Y(0), C_0)_0 = 0 \\ \forall X \in \mathcal{C}([0,t^*], L_2(\Omega)), \quad \text{and} \quad Y(t) \equiv -\displaystyle\int_t^{t^*} S^*(s-t)X(s)ds \end{array} \tag{3.12}$$

where $\mathcal{A}$ is assumed to generate a semigroup $S(t) \in \mathcal{C}([0,t^*], L_2(\Omega))$ and S^* denotes the adjoint of S in $L_2(\Omega)$. Under these assumptions, the unique weak solution to (3.7) is given by the *mild* solution (3.10) [8].

Theorem 1 *Assume that the operator $\mathcal{A}$ satisfies the uniform ellipticity condition (3.11), that $D, P, F \in L_\infty(\Omega)$ and that $\partial\Omega$ is smooth. Then $\mathcal{A}$ generates a semigroup $S(t) \in \mathcal{C}([0,\infty), L_2(\Omega))$ and satisfies $\|S(t)\| \le e^{\omega t}$ where $\omega = \|F\|_\infty^2/(4\theta)$. Also, for every $C_{\rm AIF} \in L_2([0,t^*], L_2(\Omega))$, the unique weak solution to (3.7) is given by the mild solution in (3.10).*

Proof: It will be shown that the operator $\mathcal{A}_\omega = \mathcal{A} - \omega I$ is dissipative and satisfies a range condition, and thus by the Lumer-Phillips Theorem [20] there exists a semigroup $S_\omega(t) \in \mathcal{C}([0,\infty), L_2(\Omega))$ generated by $\mathcal{A}_\omega$ and satisfying $\|S_\omega(t)\|_0 \le 1$. Then $S(t) = e^{\omega t} S_\omega(t) \in \mathcal{C}([0,\infty), L_2(\Omega))$ is the semigroup generated by $\mathcal{A}_\omega + \omega I = \mathcal{A}$ and satisfying $\|S(t)\|_0 \le e^{\omega t}$ [20]. The rest of the theorem follows as discussed in relation to (3.12) [20].

Now, dissipativity of $\mathcal{A}_\omega$ is established as follows. Note from the balanced flow assumption in Subsection 3.3 that $\nabla \cdot (F\boldsymbol{v}) = 0$ follows. Also recall from the definition of Γ and χ that $F\boldsymbol{v}^{\rm T}\boldsymbol{n}\chi = -F|\boldsymbol{v}^{\rm T}\boldsymbol{n}|\chi$. Finally, the inequality $ab \le \varepsilon^2 a^2/2 + \varepsilon^{-2} b^2/2$ is used below with $\varepsilon^2 = 2\theta$, and otherwise, the Gauss Theorem is used in the following:

$$\begin{aligned}
(\mathcal{A}_\omega C, C)_0 &= ([\nabla\cdot(\mathcal{D}\nabla C) - \nabla\cdot(F\boldsymbol{v}C) + F\boldsymbol{v}^{\rm T}\boldsymbol{n}\chi C - \omega C], C)_0 \\
&= -(\mathcal{D}\nabla C, \nabla C)_0 - ([\nabla\cdot(F\boldsymbol{v}) + F\boldsymbol{v}^{\rm T}\nabla C], C)_0 - (F|\boldsymbol{v}^{\rm T}\boldsymbol{n}|\chi C, C)_0 - \omega(C,C)_0 \\
&\le -\theta\|\nabla C\|_0^2 + \|F\|_\infty \|\nabla C\|_0 \|C\|_0 - \omega\|C\|_0^2 \\
&\le (\varepsilon^2/2 - \theta)\|\nabla C\|_0^2 + (\varepsilon^{-2}\|F\|_\infty^2/2 - \omega)\|C\|_0^2 \quad = \quad 0.
\end{aligned} \tag{3.13}$$

Then, a range condition is established for $\mathcal{A}_\omega$ as follows. It will be shown that for an arbitrary $f \in L_2(\Omega)$ and $\lambda > \omega$, there exists a unique $C \in {\rm Dom}(\mathcal{A})$ such that $[\lambda - \mathcal{A}_\omega]C = f$ or:

$$\left\{ \begin{array}{rcll} -\nabla\cdot(\mathcal{D}\nabla C) + \nabla\cdot(F\boldsymbol{v}C) + F|\boldsymbol{v}^{\rm T}\boldsymbol{n}|\chi C + (\omega+\lambda)C &=& f, & \Omega \\ \boldsymbol{n}^{\rm T}\mathcal{D}\nabla C &=& 0, & \partial\Omega. \end{array} \right. \tag{3.14}$$

For this, define the bilinear form on $H^1(\Omega) \times H^1(\Omega)$:

$$B(\phi,\psi) = (\mathcal{D}\nabla\phi, \nabla\psi)_0 + (F\boldsymbol{v}^{\rm T}\nabla\phi, \psi)_0 + (F|\boldsymbol{v}^{\rm T}\boldsymbol{n}|\chi\phi, \psi)_0 + (\omega+\lambda)(\phi,\psi)_0 \tag{3.15}$$

and the linear form on $H^1(\Omega)$:

$$L(\phi) = (f, \phi)_0. \tag{3.16}$$

Both forms are bounded:

$$\begin{aligned}
|B(\phi,\psi)| &\le \max\{\|D\|_\infty, \|P\|_\infty\}\|\nabla\phi\|_0\|\nabla\psi\|_0 + \|F\|_\infty\|\nabla\phi\|_0\|\psi\|_0 + (\|F\|_\infty + \omega)\|\psi\|_0 \\
&\le \max\{\|D\|_\infty, \|P\|_\infty, \|F\|_\infty + \omega\}\|\phi\|_1\|\psi\|_1 \\
|L(\phi)| &\le \|f\|_0\|\phi\|_0 \quad \le \quad \|f\|_0\|\phi\|_1.
\end{aligned} \tag{3.17}$$

Using $\varepsilon^2 = \theta$ in the following shows the coercivity of the bilinear form:

$$\begin{aligned}
B(\phi,\phi) &\ge \theta\|\nabla\phi\|_0^2 - \|F\|_\infty\|\nabla\phi\|_0\|\phi\|_0 + \omega\|\phi\|_0^2 \\
&\ge (\theta - \varepsilon^2/2)\|\nabla\phi\|_0^2 + (\omega + \lambda - \varepsilon^{-2}\|F\|_\infty^2/2)\|\phi\|_0^2 \\
&\ge \min\{\theta/2, \lambda - \omega\}\|\phi\|_1^2.
\end{aligned} \tag{3.18}$$

Thus, by the Lax-Milgram Lemma, there exists a unique weak solution C to (3.14) [12]. As shown in [17], given the smoothness of $\partial\Omega$ and the assumed properties of the coefficients in (3.14), the solution C actually possesses the additional regularity:

$$\|C\|_2 \le c\|f\|_0 \tag{3.19}$$

and thus $C \in {\rm Dom}(\mathcal{A})$ and $[\lambda - \mathcal{A}_\omega]C = f$. ∎

3.6 The Convolution Model

Under the assumption that the initial concentration in Ω is zero, C_{T} and C_{AIF} are related by a convolution,

$$C_{\mathrm{T}}(t) = \int_0^t K(t-s) C_{\mathrm{AIF}}(s) ds \tag{3.20}$$

with a kernel K which through (3.4) may be considered for large S as the limit of kernels of the form:

$$K(t) \leftarrow \boldsymbol{e}^{\mathrm{T}} V \exp[V^{-1} A t] V^{-1} \boldsymbol{b} / \boldsymbol{e}^{\mathrm{t}} V \boldsymbol{e} = \boldsymbol{e}^{\mathrm{T}} \exp[A V^{-1} t] \boldsymbol{b} / \boldsymbol{e}^{\mathrm{t}} V \boldsymbol{e} \tag{3.21}$$

or through (3.10) for vanishing support of χ as the limit of kernels of the form:

$$K(t) \leftarrow \int_\Omega S(t) \mathcal{B} d\boldsymbol{x} / \mathrm{vol}(\Omega) = \int_\Omega S(t) F |\boldsymbol{v}^{\mathrm{T}} \boldsymbol{n}| \chi d\boldsymbol{x} / \mathrm{vol}(\Omega). \tag{3.22}$$

For an impulsive arterial input $C_{\mathrm{AIF}}(t) = \delta(t)$ the kernel may be seen to give the tissue impulse response $C_{\mathrm{T}}(t) = K(t)$, a concentration course which is non-increasing and which vanishes as the contrast agent clears from Ω; see Appendix B. Physiological parameters associated with the kernel may be derived by integrating (3.1) and applying the Gauss Theorem to obtain:

$$\mathrm{vol}(\Omega) C_{\mathrm{T}}(t) = \int_\Omega C(t) d\boldsymbol{x} = \int_{\boldsymbol{v}^{\mathrm{T}} \boldsymbol{n} < 0} F |\boldsymbol{v}^{\mathrm{T}} \boldsymbol{n}| d\boldsymbol{x} \int_0^t C_{\mathrm{AIF}}(s) ds - \int_{\boldsymbol{v}^{\mathrm{T}} \boldsymbol{n} > 0} F |\boldsymbol{v}^{\mathrm{T}} \boldsymbol{n}| d\boldsymbol{x} \int_0^t C_{\mathrm{VOF}}(s) ds \tag{3.23}$$

since F and $\boldsymbol{v}$ are assumed to be time-independent and since diffusive flux at $\partial\Omega$ is assumed negligible.

The significance of the initial value $K(0)$ is found by inserting $C_{\mathrm{AIF}}(t) = \delta(t)$ and taking the limit in (3.23) toward the initial time, when $C_{\mathrm{VOF}}(0) = 0$, to find the volumetric flow rate $\int_{\boldsymbol{v}^{\mathrm{T}} \boldsymbol{n} < 0} F |\boldsymbol{v}^{\mathrm{T}} \boldsymbol{n}| d\boldsymbol{x}$ (volume/time) on the right and $\mathrm{vol}(\Omega) K(0)$ on the left, where:

$$\mathcal{F}_{\mathrm{T}} = K(0) = \frac{1}{\mathrm{vol}(\Omega)} \int_{\boldsymbol{v}^{\mathrm{T}} \boldsymbol{n} < 0} F |\boldsymbol{v}^{\mathrm{T}} \boldsymbol{n}| d\boldsymbol{x} \tag{3.24}$$

(1/time) is the *volumetric flow rate per unit tissue volume*. The normalized function $R(t) = K(t)/K(0)$ is called the *residue function*, as it represents the fraction of contrast agent which has not yet cleared from the tissue.

The residue function is related as follows to the *mean transit time*. Because the flow through Ω is assumed to be balanced, $\int_{\boldsymbol{v}^{\mathrm{T}} \boldsymbol{n} < 0} F |\boldsymbol{v}^{\mathrm{T}} \boldsymbol{n}| d\boldsymbol{x} = \int_{\boldsymbol{v}^{\mathrm{T}} \boldsymbol{n} > 0} F |\boldsymbol{v}^{\mathrm{T}} \boldsymbol{n}| d\boldsymbol{x}$ holds. Since C_{AIF} and C_{VOF} are assumed spatially constant, it follows from (3.20), (3.23), and (3.24) that $[R * C_{\mathrm{AIF}}]'(t) = C_{\mathrm{AIF}}(t) - C_{\mathrm{VOF}}(t)$. Thus, C_{AIF} and C_{VOF} are related by the convolution $C_{\mathrm{VOF}}(t) = [C_{\mathrm{AIF}} * h](t)$ where $R(t) = \int_t^\infty h(s) ds$. When h is interpreted as the probability density of the transit time of a contrast agent particle through Ω, the mean transit time is given by:

$$\mathcal{T}_{\mathrm{T}} = \int_0^\infty t h(t) dt = \int_0^\infty R(t) dt = \int_0^\infty \frac{K(t)}{K(0)} dt. \tag{3.25}$$

The volume fraction of Ω in which contrast agent is distributed is now obtained by inserting $C_{\mathrm{AIF}}(t) = \delta(t)$ and $C_{\mathrm{VOF}} = h(t)$ into (3.23) to find $R(t) \int_{\boldsymbol{v}^{\mathrm{T}} \boldsymbol{n} < 0} F |\boldsymbol{v}^{\mathrm{T}} \boldsymbol{n}| d\boldsymbol{x}$ on the right and $\mathrm{vol}(\Omega) K(t)$ on the left. Integrating for all times and using (3.25) gives $\mathcal{T}_{\mathrm{T}} \int_{\boldsymbol{v}^{\mathrm{T}} \boldsymbol{n} < 0} F |\boldsymbol{v}^{\mathrm{T}} \boldsymbol{n}| d\boldsymbol{x}$ on the right. This product of mean transit time and volumetric flow rate gives the effective volume within Ω in which contrast agent is distributed. Therefore, the *effective volume fraction* is:

$$\mathcal{V}_{\mathrm{T}} = \int_0^\infty K(t) dt = \frac{\mathcal{T}_{\mathrm{T}}}{\mathrm{vol}(\Omega)} \int_{\boldsymbol{v}^{\mathrm{T}} \boldsymbol{n} < 0} F |\boldsymbol{v}^{\mathrm{T}} \boldsymbol{n}| d\boldsymbol{x} = \mathcal{T}_{\mathrm{T}} \mathcal{F}_{\mathrm{T}}. \tag{3.26}$$

The reader familiar with the literature concerning the association between kernel parameters and transport properties, e.g., [10], [11], [15], [18], [23], may be questioning at this point which

types of examinations or tracers are characterized by (3.24), (3.25) and (3.26). The answer is that the present analysis applies to *all* applications in which tracer is transported passively by convection and diffusion and the assumptions of Subsection 3.3 are satisfied.

On the other hand, the tissue transport states described in Section 1 may be associated with the *spectral* properties of the convolution kernel as follows on the basis of the detailed results shown in Appendix B. For pure convection the eigenvalues of $V^{-1}A$ are clustered, and the representative kernel is a sum of Erlang distributions. In the ischemic limit that flow is limited to a narrow convective chain, an Erlang distribution leads to a step function representation of a plug flow. On the other hand, high vascularization increases the variance in the eigenvalue cluster. For pure streamline oriented diffusion, the eigenvalues of $V^{-1}A$ are widely distributed, and the representative kernel is a sum of decaying exponential functions. In the limit of high diffusivity, all but one eigenvalue of $V^{-1}A$ give negligibly transient dynamics and the smallest eigenvalue leads to a mono-exponential kernel. For pure permeation oriented diffusion, the eigenvalues of $V^{-1}A$ are widely distributed and can easily be complex. Such eigenvalues make the representative kernel a sum of products of trigonometric and decaying exponential functions, which corresponds to recirculation of contrast agent through Ω.

3.7 Nonidentifiability

Thus, on the basis of the results presented in Appendix B, the most physiologically meaningful basis with which to represent the desired kernel might consist of the span of decaying exponential functions, products between polynomials and decaying exponentials, and products between trigonometric and decaying exponential functions. Ideally, when a kernel is estimated from the span of such functions, the weights of these different types of span elements might be correlated to the respective tissue transport states described in Appendix B. However, the following theorem shows that a kernel which could correspond to any one of these states may be approximated arbitrarily well by a purely convective kernel, and thus these different tissue transport states cannot be decided on the basis of the kernel alone; see also the illustration in Fig. 1. Here and in Appendix B, $\text{tridiag}\{b_i, a_i, c_i\} \in \boldsymbol{R}^{N\times N}$ denotes the tridiagonal matrix with sequential elements $\{b_i, a_i, c_i\}$ in the ith row and $b_1 = c_N = 0$. Also, $\boldsymbol{\epsilon}, \boldsymbol{\epsilon}_i \in \boldsymbol{R}^N$ denote the vectors $\boldsymbol{\epsilon} = \langle 1, 1, \ldots, 1\rangle^{\mathrm{T}}$ and $\boldsymbol{\epsilon}_i = \langle 0_1, \ldots, 1_i, \ldots, 0_N\rangle^{\mathrm{T}}$. Note that the assumption $\int_0^\infty K(t)dt \leq 1$ in the following is natural since $\mathcal{V}_\mathcal{T}$ in (3.26) is the effective volume *fraction*.

Theorem 2 *Suppose that $K(t) \in L_1[0,\infty)$ is non-negative and non-increasing and satisfies $\int_0^\infty K(t)dt \leq 1$, and suppose that a constant $\text{vol}(\Omega)$ is given. Then K can be approximated arbitrarily well in $L_1[0,\infty)$ for sufficiently large N, M, $S = N \times (M+1)$ by $\boldsymbol{e}^{\mathrm{T}} \exp[AV^{-1}t]\boldsymbol{b}/\boldsymbol{e}^{\mathrm{T}}V\boldsymbol{e}$ where V is a block diagonal matrix $\text{diag}\{V_m I\}_{m=0}^M$ with $N \times N$ diagonal blocks $V_m I$, $V_m > 0$, satisfying $\boldsymbol{e}^{\mathrm{T}}V\boldsymbol{e} = \text{vol}(\Omega)$, A is a block diagonal matrix $\text{diag}\{A_m\}_{m=0}^M$ with $N\times N$ lower bidiagonal blocks $A_m = \text{tridiag}\{k_m, -k_m, 0\}$, $k_m > 0$, and $\boldsymbol{b}$ is the concatenation $\{k_m\boldsymbol{\epsilon}_1\}_{m=0}^M$ of vectors $k_m\boldsymbol{\epsilon}_1 \in \boldsymbol{R}^N$.*

Proof: The claim is proved by first constructing a sequence of simple functions which converges to the given kernel. Then it is shown that each of these simple functions may be approximated by a weighted sum of Erlang functions (corresponding physiologically to parallel convective tubes) which can be written in the exponential form stated above.

For a given positive integer L, define $t_m = \sup\{t : K(t) \geq m/2^L\}$, $m = 1, \ldots, M_L$, where M_L is the largest integer satisfying $0 < M_L/2^L \leq \min\{L, K(0)\}$. Then define the associated step functions $\rho(t - t_m) = \int_t^\infty \delta(s - t_m)ds$ and the simple function:

$$K_L(t) = \sum_{m=1}^{M_L} [K(t_m) - K(t_{m-1})]\rho(t - t_m) \tag{3.27}$$

with the understanding that $K(t_0) = 0$. Since $\{K_L\}$ is an increasing sequence of simple functions such that $K_L \to K$ a.e. while each $K_L \geq 0$ is dominated by $K \geq 0$, K_L converges to K in

$L_1[0,\infty)$ as $L \to \infty$ by the Dominated Convergence Theorem; see the related construction on p. 38 in [1].

Given the values $\{t_m\}_{m=1}^{M_L}$ and a positive integer N, define $k_m = [K(t_m) - K(t_{m-1})]\mathrm{vol}(\Omega)$ and $V_m = k_m t_m/N$ for $1 \le m \le M_L$, and note that $N\sum_{m=1}^{M_L} V_m = \mathrm{vol}(\Omega)\int_0^\infty K_L(t)dt$. For $m = 0$, set $V_0 = (\mathrm{vol}(\Omega)/N)[1 - \int_0^\infty K_L(t)dt]$ and $k_0 = 0$ (so that the subregions with volume V_0 are inaccessible by passive transport). Then let V be the block diagonal matrix $\mathrm{diag}\{V_m I\}_{m=0}^{M_L}$ with $N \times N$ diagonal blocks $V_m I$, and note that:

$$\boldsymbol{e}^{\mathrm{T}} V \boldsymbol{e} = NV_0 + N\sum_{m=1}^{M_L} V_m = \mathrm{vol}(\Omega)\left[1 - \int_0^\infty K_L(t)dt\right] + \mathrm{vol}(\Omega)\int_0^\infty K_L(t)dt = \mathrm{vol}(\Omega). \quad (3.28)$$

Now let A be the block diagonal matrix $\mathrm{diag}\{A_m\}_{m=0}^{M_L}$ with $N \times N$ lower bidiagonal blocks $A_m = \mathrm{tridiag}\{k_m, -k_m, 0\}$, and let $\boldsymbol{b}$ be the concatenation $\{k_m\boldsymbol{\epsilon}_1\}_{m=0}^{M_L}$ of vectors $k_m\boldsymbol{\epsilon}_1 \in \boldsymbol{R}^N$. Then the following holds:

$$\frac{\boldsymbol{e}^{\mathrm{T}} \exp\left[AV^{-1}t\right]\boldsymbol{b}}{\boldsymbol{e}^{\mathrm{T}} V \boldsymbol{e}} = \sum_{m=1}^{M_L} \boldsymbol{\epsilon}^{\mathrm{T}} \exp\left[A_m t/V_m\right]\boldsymbol{\epsilon}_1 \frac{k_m}{\mathrm{vol}(\Omega)} = \sum_{m=1}^{M_L} [K(t_m) - K(t_{m-1})]R_m(t) \quad (3.29)$$

where $\boldsymbol{\epsilon}^{\mathrm{T}} \exp[A_m t/V_m]\boldsymbol{\epsilon}_1$ is the Erlang function $R_m(t) = \sum_{n=0}^{N-1}(Nt/t_m)^n/n!$ which converges in $L_1[0,\infty)$ to the step function $\rho(t - t_m)$ as $N \to \infty$. Thus, for L sufficiently large, (3.27) is sufficiently close to K, and for $N = N(L)$ sufficiently large, (3.29) is sufficiently close to (3.27). Therefore, (3.29) satisfies the conditions of the theorem. ∎

For a simple illustration of Theorem 2, consider the examples of Fig. 1. Recall that the exchange between compartments in Fig. 1a is purely convective while the exchange between compartments in Fig. 1b is also diffusive. Yet the parameters in (3.2) may be chosen so that their respective residue functions are identical. It follows in general from Theorem 2 that unless tissues can be shown to satisfy special assumptions, made for the development of models such as [10], [11], and [18], tissue transport states cannot in general be identified on the basis of a single convolution equation. In spite of the limitations imposed by the assumptions made to arrive at a given convolution model, (3.20) is a useful formulation for DCE-MRI and it is applied in [14] to estimate the physiological parameters given in (3.24), (3.25), and (3.26).

4 Conclusion

In this paper the need for a revision in the theory of tracer transport and the convolution model of DCE-MRI has been presented along with a new foundation based upon a fully distributed convection-diffusion model. Compartmental discretizations and alternatively semigroup theory has been used to freshly derive familiar mathematical relations while illuminating their limits of applicability. Principal among the assumptions emerging in this analysis is that the construction of the convolution model depends upon there being no diffusive coupling between the selected tissue region and its surroundings. Also it was found important to assume that there are no convective sources in the tissue, that the tissue properties exhibit stationarity, and that the input and output concentrations are spatially constant. On the basis of the detailed results given in the appendices, distinct tissue transport states are related to the fully distributed model and to the spectral properties of the convolution kernel. However, it has been shown in this work that these tissue transport states cannot be identified from the convolution kernel alone. Nevertheless, nonparametric regularized deconvolution methods for kernel estimation are presented in the follow-up work [14], although their applicability is naturally constrained by the theoretical results reported here.

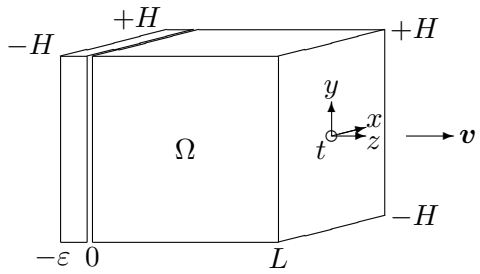

Figure 3: Simple geometry for the solution of the convection diffusion equation (3.1).

A Solutions for the Distributed Parameter Model

In this appendix a simple geometry is defined and explicit solutions to the convection-diffusion equation (3.1) are discussed; see [6] for further details on the construction of such classical solutions. Consider the geometry as shown in Fig. 3. Assume that Ω lies in the rectangular region $-H \leq x, y \leq H$, $0 < z < L$ with inflow and outflow boundaries respectively located at $z = 0$ and $z = L$. Suppose here, in contrast to Appendix B, that the concentration flux at the boundary $\partial\Omega$ is not necessarily purely convective. Assume further that $\boldsymbol{v} = \boldsymbol{e}_z$ is a constant vector field everywhere aligned with the z-axis. To generate a nearly impulsive influx let the initial concentration be given by $C_0(x, y, z) = \chi_{[-H,+H]}(x)\chi_{[-H,+H]}(y)\chi_{[-\varepsilon,0]}(z)$, where χ_S denotes the characteristic function vanishing outside the set S.

A.1 Pure Convection

First assume that transport is purely convective so that $D = P = 0$ holds. Assume also that the mean velocity $F = F(x, y)$ is a function only of (x, y). The solution to (3.1) is given by:

$$C(x, y, z, t) = C_0(x, y, z - F(x, y)t). \tag{A.1}$$

To model ischemia, let $F(x, y)$ be supported on a very narrow interval $|x|, |y| \leq \delta$, so that $F(x, y)$ is essentially the constant F_0 on its support. Then the influx wave propagates to the outflow boundary of Ω and arrives and exits at the times $t_{\mathrm{a}} = L/F_0$ and $t_{\mathrm{e}} = (L + \varepsilon)/F_0$, respectively. On the other hand, to model high vascularization let $F(x, y)$ have broad support and variation. Then the influx wave undergoes considerable dispersion and reaches the outflow boundary at a great variety of arrival and exit times $t_{\mathrm{a}} = L/F(x, y)$ and $t_{\mathrm{e}} = (L + \varepsilon)/F(x, y)$. The same qualitative result is also achieved for a constant mean velocity F when the unit vector field $\boldsymbol{v}$ is not constant and generates trajectories of greatly varying lengths in Ω.

A.2 Streamline Oriented Diffusion

Now assume that transport is streamline oriented diffusion dominated or that $D > 0$ and $P = 0$ hold. The solution to (3.1) is given by:

$$\begin{aligned} C(x, y, z, t) &= \int_{-\infty}^{+\infty} \frac{C_0(x, y, \zeta)}{\sqrt{4\pi D t}} \exp\left[-\frac{(z - \zeta - F(x, y)t)^2}{4Dt}\right] d\zeta \\ &= \frac{1}{2}\mathrm{erf}\left[\frac{F(x, y)t - z}{\sqrt{4Dt}}\right] - \frac{1}{2}\mathrm{erf}\left[\frac{F(x, y)t - z - \varepsilon}{\sqrt{4Dt}}\right]. \end{aligned} \tag{A.2}$$

As D vanishes, the solution takes a square wave form for fixed (x, y) as seen in (A.1). For $D > 0$, the square wave is smoothed in the z direction and has full support on the z-axis. Therefore, since $C(x, y, L, t)$ is positive for all t, infinite time is required for the contrast agent to clear Ω.

A.3 Permeation Oriented Diffusion

Now assume that transport is permeation oriented diffusion dominated or that $P > 0$ and $D = 0$ hold. For simplicity, assume that the mean velocity F is everywhere constant. The solution to (3.1) is given by:

$$C(x,y,z,t) = \int_{-\infty}^{+\infty}\int_{-\infty}^{+\infty} \frac{C_0(\xi,\eta,z-Ft)}{4\pi Pt} \exp\left[-\frac{(x-\xi)^2+(y-\eta)^2}{4Pt}\right] d\xi d\eta = \tag{A.3}$$
$$\chi_{[-\varepsilon,0]}(z-Ft)\left\{\frac{1}{2}\mathrm{erf}\left[\frac{x+H}{\sqrt{4Pt}}\right] - \frac{1}{2}\mathrm{erf}\left[\frac{x-H}{\sqrt{4Pt}}\right]\right\}\left\{\frac{1}{2}\mathrm{erf}\left[\frac{y+H}{\sqrt{4Pt}}\right] - \frac{1}{2}\mathrm{erf}\left[\frac{y-H}{\sqrt{4Pt}}\right]\right\}.$$

As P vanishes, the solution takes the square wave form seen in (A.1). For $P > 0$, the square wave is smoothed in the x and y directions and has full support in the (x, y) plane. However, with a constant unit vector field $\boldsymbol{v}$ in this case, the wave always clears Ω in finite time because of the factor $\chi_{[-\varepsilon,0]}(z - Ft)$. On the other hand, when the unit vector field $\boldsymbol{v}$ is not constant, a positive curvature zone in a convective pathway allows counter-current exchange, and the contrast agent can move upstream by permeation oriented diffusion alone. Such flows thereby exhibit recirculation of contrast agent and infinite clearance times. Finally, note that the extraction fraction $E = [C_{\mathrm{AIF}}(0) - C_{\mathrm{VOF}}(t_{\mathrm{a}})]/C_{\mathrm{AIF}}(0)$ can be derived from (A.3) by inserting the arrival time $t_{\mathrm{a}} = L/F$ at the outflow boundary $(x, y, z) = (0, 0, L)$ to obtain the ratio $E = 1 - \mathrm{erf}\{[\frac{H^2}{4P}\frac{F}{L}]^{\frac{1}{2}}\}^2$, which is qualitatively similar to the exponential factor derived in [21] for an idealized single capillary.

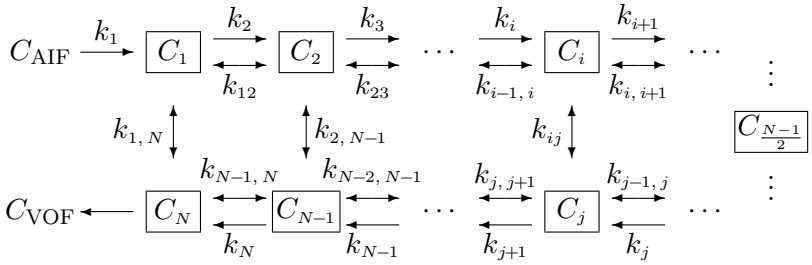

Figure 4: A chain of compartments connecting the arterial input with the venous output, where the constants k_i are purely convective and the constants k_{ij} are purely diffusive.

B Solutions for the Compartmental Model

In this appendix the compartment models leading to qualitatively distinct convolution kernels appearing in (3.4) are summarized. A kernel of the form shown in (3.4), based upon a finite number of compartments, must be consistent with (3.1) in the sense that compartment refinement leads to a limit kernel in (3.20) which is equal to $[\mathrm{vol}(\Omega)]^{-1}\int_\Omega C(t)d\boldsymbol{x}$ when the arterial input is impulsive and the flux at $\partial\Omega$ is purely convective. Nevertheless, the primary goal here is to differentiate between underlying compartment models in (3.4) on the basis of their spectral properties.

For the following examples, consider the compartment model shown in Fig. 4, which is a spatial integration through Ω of a convective tube aligned with the vector field $\boldsymbol{v}$. For simplicity, this example admits the possibility of direct counter-current exchange across a stagnation surface as opposed to a system of intermediate subregions. The constants k_i and k_{ij} are as described in relation to (3.2). From the discretization of (3.1), each of these constants depends upon geometric parameters such as surface areas. Also, the convective constants k_i depend on the mean velocity F, the diffusive constants k_{ij} inside the convective pathway depend upon the diffusivity D, and the diffusive constants outside the convective pathway depend upon the

diffusivity P. This spatial discretization of (3.1) is written in (3.2) and (3.3), with $\boldsymbol{b} = k_1\boldsymbol{\epsilon}_1$ and $A = A_F + A_{\mathcal{D}}$, $A_{\mathcal{D}} = A_D + A_P$, where A_F includes the convective constants, A_D includes the diffusive constants inside the convective pathway, and A_P includes the diffusive constants outside the convective pathway. The solution to this system can be written in the forms (3.4) and (3.20) with $\boldsymbol{e} = \boldsymbol{\epsilon}$ in (3.21). Here, the kernel (3.22) is necessarily decaying since $\Re\{\sigma(V^{-1}A)\} < 0$ follows from the fact that $V^{-1}A$ is irreducibly diagonally dominant with negative diagonal entries [24].

B.1 Pure Convection

Now assume that transport is purely convective so that $D = P = 0$ holds, and the constants in Fig. 4 satisfy $A_{\mathcal{D}} = 0$ and $A = A_F = \text{tridiag}\{k_i, -k_i, 0\}$. Since A is lower triangular, it has eigenvalues $\{-k_i\}$. Further, if the flow is balanced throughout the chain and the compartment volumes are equal, then A has a single eigenvalue $-k_1$ of multiplicity N and (3.22) leads to the Erlang distribution $R(t) = e^{-k_1 t/V_1}\sum_{n=0}^{N-1}(k_1 t/V_1)^n/n!$ for the residue function. From the dependence of k_1 on geometry, NV_1/k_1 converges as $N \to \infty$ to a constant which is $\mathcal{T}_{\text{T}}$. Thus, $R(t)$ converges to the step function $\int_t^\infty \delta(s-\mathcal{T}_{\text{T}})ds$ and $h(t)$ to the delta function $\delta(t-\mathcal{T}_{\text{T}})$. Even if the eigenvalues of $V^{-1}A$ are distinct, their accumulation near a point depending upon the average among mean velocities implies a representative kernel consisting of a sum of products between polynomials and decaying exponentials.

B.2 Streamline Oriented Diffusion

Now assume that transport is streamline oriented diffusion dominated or that $D > 0$ and $P = 0$ hold. Then diffusion is only lengthwise in the convective chain of Fig. 4, and the constants satisfy $A_P = 0$ and $A = A_F + A_D$, with $A_F = \text{tridiag}\{k_i, -k_i, 0\}$ and $A_D = \text{tridiag}\{k_{i,i-1}, -k_{i,i-1} - k_{i,i+1}, k_{i,i+1}\}$. Here, A_D approximates an elliptic operator with Neumann boundary conditions which rule out diffusive flux at the chain boundary as assumed in (3.20). Since the two off-diagonals of $V^{-1}A$ have all positive elements, $V^{-1}A$ is symmetrizable [9], and thus its spectrum is real. From $\Re\{\sigma(V^{-1}A)\} < 0$ it follows that $\sigma(V^{-1}A) < 0$. In the limit that $A \approx A_F$ holds, the qualitative properties of $K(t)$ are as described earlier for pure convection. In the opposite limit that $A \approx A_D$ holds, A_D has a smoothing effect on $V^{-1}A$ and it spreads an otherwise concentrated spectrum of $V^{-1}A_F$. To see this, assume for simplicity that $V_i = V_1$ so that $V^{-1}A = A/V_1$. Suppose further that $k_i = k_1$ and $k_{i,i+1} = k_{12}$ hold, where significant dependencies of k_1 and k_{12} can be expressed as $k_1/V_1 = \mathcal{O}(F)\mathcal{O}(N)$ and $k_{12}/V_1 = \mathcal{O}(D)\mathcal{O}(N^2)$. A discrete cosine transform T diagonalizes A_D to $T^{-1}A_D T = 2k_{12}\text{diag}\{\cos[\pi(i-1)/N] - 1\}$ [22]. By the Gerschgorin Theorem [24], the spectrum of A is an $\mathcal{O}(F)$ perturbation of that of A_D, and thus for sufficiently large D, A has distinct eigenvalues spread over a negative real interval of length $\mathcal{O}(D)$. Since zero is always in the spectrum of A_D, the eigenvalue of A with the least magnitude is an $\mathcal{O}(F)$ perturbation of zero and thus it has the least transient effect on $K(t)$. To estimate this eigenvalue $\lambda_1(D)$ as $D \to \infty$, let $\boldsymbol{x}_1(D)$ be the corresponding eigenvector normalized so that $\|\boldsymbol{x}_1(D)\|_2 = 1$. For large D it follows from $D^{-1}A_D\boldsymbol{x}_1(D) \approx D^{-1}(A_F + A_D)\boldsymbol{x}_1(D) = D^{-1}\lambda_1(D)\boldsymbol{x}_1(D) \approx 0$ that $\boldsymbol{x}_1(D) \to \boldsymbol{\epsilon}/\sqrt{N}$ as $D \to \infty$. From $\lambda_1(D) = \boldsymbol{x}_1(D)^{\text{T}}(A_F + A_D)\boldsymbol{x}_1(D) = \boldsymbol{x}_1(D)^{\text{T}}A_F\boldsymbol{x}_1(D)$, it follows that $\lambda_1(D) \to -k_1/N$ as $D \to \infty$, and the effect on $K(t)$ of the other eigenvalues of A becomes negligibly transient. Thus, $-V_1/\lambda_1(D) \approx NV_1/k_1 \to \mathcal{T}_{\text{T}}$ as $N \to \infty$. Since $\boldsymbol{x}_1(D)$ has identical components, it follows that in the diffusive limit, all compartments in the chain are instantly brought to the same concentration and may be considered as a single well mixed compartment with a mono-exponential kernel $\mathcal{T}_{\text{T}}^{-1}e^{-t/\mathcal{T}_{\text{T}}}$. As the diffusion level is reduced, the next larger eigenvalues become less transient and add additional exponential functions to create a sum of decaying exponentials for the kernel.

B.3 Permeation Oriented Diffusion

Now assume that transport is permeation oriented diffusion dominated or that $P > 0$ and $D = 0$ hold. Before considering the full compartment chain shown in Fig. 4, let $N = 1$ and otherwise construct a planar array of parallel compartments between C_{AIF} and C_{VOF}. For such an array, $A = A_F + A_P$ where A_F is diagonal and A_P approximates an elliptic operator with Neumann boundary conditions which rule out diffusive flux at the planar array boundary as assumed in (3.20). The inequality $\Re\{\sigma(V^{-1}A)\} < 0$ implies that $K(t)$ in (3.22) is necessarily decreasing, and it follows from the form $K(t) = \boldsymbol{e}^{\mathrm{T}} V^{\frac{1}{2}} \exp[V^{-\frac{1}{2}} A V^{-\frac{1}{2}} t] V^{-\frac{1}{2}} \boldsymbol{b} / \boldsymbol{e}^{\mathrm{T}} V \boldsymbol{e}$ that the necessarily real eigenvalues of the symmetric matrix $V^{-\frac{1}{2}} A V^{-\frac{1}{2}}$ are negative. Thus, using analysis such as in the last subsection, it can be shown that the kernel consists of a single decaying exponential when the planar array is well mixed or else a sum of decaying exponentials depending upon the magnitude of the next eigenvalues. When this planar array is placed in series for $N > 1$, an N-fold convolution of the unit kernel leads to Erlang distributions and then step functions as discussed for the pure convection case. On the other hand, permeability leads as follows to qualitative behavior distinct from the cases discussed so far. Assume in Fig. 4 that $N > 1$ and that $A_D = 0$. Then the non-zero constants appearing in $A_F + A_P$ can be chosen quite naturally to generate complex eigenvalues for A; e.g., let $\kappa = 1$, $\nu = 1$, and $\rho = 1/2$ in Fig. 5. The resulting sums of products between trigonometric and decaying exponential functions corresponds to contrast agent recirculation in Fig. 4. In fact, conspicuous oscillations can result in C_1 and C_N from an impulsive input when, particularly for large N, $k_{1,N}$ is the only positive diffusive constant. Nevertheless, the total sum in (3.22) is decreasing.

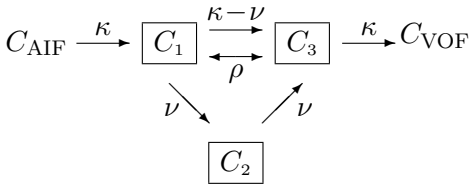

Figure 5: A compartment network implicitly incorporating arbitrarily oriented diffusion at convective pathway branch points.

B.4 General Compartment Networks

Recall that the characterizations above are reached by deriving the compartment network in Ω from spatially integrating the unit vector field $\boldsymbol{v}$. Consider now a completely general compartment network constrained only by the requirement that convective links never point from higher to lower pressure compartments. Then when compartments are numbered from highest to lowest pressure, the resulting A_F is lower triangular. Consequently, the conclusions drawn above for the pure convection case are reached again; moreover, it may be emphasized additionally here that the scatter of convective constants, or equivalently of system eigenvalues, can range from narrow, in the case of ischemia, to diffuse, in the case of high vascularization. Next, since real or complex, accumulated or distributed eigenvalues are realized by the compartment models described earlier for pure permeation oriented diffusion, the associated qualitative behavior is also obtained for more general networks. Finally, consider the compartment model shown in Fig. 5. With $\kappa = 1$, $\nu = 3/4$, and $\rho = 1/4$, A has complex eigenvalues. The definitions given earlier for the diffusive constants inside and outside the convective pathway imply now that $A_P = 0$ and $A = A_F + A_D$ hold, and the emergence of complex eigenvalues here contrasts with the characterization reached earlier for pure streamline oriented diffusion. However, as compartments are always assumed to be well mixed, the compartments defined in Fig. 5 implicitly incorporate arbitrarily oriented diffusion at branch points in the convective pathway.

In particular, permeation oriented diffusion is implicitly in effect inside compartments 1 and 3 even though only streamline oriented diffusion is defined explicitly between these compartments. It may be concluded that the complex eigenvalues emerging in Fig. 5 result from permeation oriented diffusion, and that streamline oriented diffusion is characterized as shown above by widely distributed real eigenvalues.

References

[1] R.B. Ash, *Real Analysis and Probability*, Academic Press, New York, 1972.

[2] H.T. Banks and P. Kareiva, *Parameter Estimation Techniques for Transport Equations with Application to Population Dispersal and Tissue Bulk Flow Models*, J. Math. Biology, Vol. 17, pp. 253–273, 1983.

[3] H.T. Banks and K. Kunisch, *Estimation Techniques for Distributed Parameter Systems*, Birkhäuser, Boston, 1989.

[4] G.K. Batchelor, *An Introduction to Fluid Dynamics*, Cambridge Univ. Press, Cambridge, 1990.

[5] F. Calamante, D.G. Gadian, A. Connelly, *Quantification of Bolus Tracking MRI: Improved Characterization of the Tissue Residue Function using Tikhonov Regularisation*, Magn. Reson. Med., Vol. 50, No. 6, pp. 1237–1247, 2003.

[6] H.S. Carslaw and J.C. Jaeger, *Conduction of Heat in Solids*, Clarendon Press, Oxford, 1959.

[7] E. Carson and C. Cobelli, *Modeling Methodology for Physiology and Medicine*, Academic Press, 2000.

[8] R.F. Curtain and A.J. Pritchard, *Infinite Dimensional Linear Systems Theory*, Springer-Verlag, Berlin, 1978.

[9] H.C. Elman, G.H. Golub, *Iterative Method for Cyclically Reduced Non-Self-Admoint Linear Systems*, Math. Comput., Vol. 54, pp. 671–700, 1990.

[10] J. Griebel, S. Pahernik, R. Lucht, A. DeVries, K.-H. Englmeier, M. Dellian, G. Brix, *Perfusion and Permeability: Can Both Parameters Be Evaluated Separately from Dynamic MR Data?*, Proc. Intl. Soc. Mag. Reson. Med. 9, 2001.

[11] E. Henderson, J.S. Sykes, D. Drost, H.-J. Weinmann, B.K. Rutt, T.-Y. Lee, *Simultaneous MRI Measurement of Blood Flow, Blood Volume, and Capillary Permeability in Mammary Tumors Using Two Different Contrast Agents*, J. Magn. Reson. Imaging, Vol. 12, pp. 991–1003, 2000.

[12] V. Hudson and J.S. Pym, *Applications of Functional Analysis and Operator Theory*, Academic Press, London, 1980.

[13] S.L. Keeling, R. Bammer, T. Kogler and R. Stollberger, *On the Convolution Model of Dynamic Contrast Enhanced Magnetic Resonance Imaging and Nonparametric Deconvolution Approaches*, Special Research Center Report 298, University of Graz, Austria, 2004.

[14] S.L. Keeling, T. Kogler and R. Stollberger, *Nonparametric Deconvolution Approaches to Dynamic Contrast Enhanced Magnetic Resonance Imaging*, submitted to Medical Image Analysis.

[15] S.S. Kety, *The Theory and Applications of the Exchange of Inert Gas at the Lungs and Tissues*, Pharmacol. Rev. Vol. 3, pp. 1–41, 1951.

[16] T.S. Koh, L.H. Cheong, and Y.C. Soh, *A Physiologic Model of Capillary-Tissue Exchange for Dynamic Contrast-Enhanced Imaging of Tumor Microcirculation*, IEEE Trans. on Biomed. Eng., Vol. 50, No. 2, pp. 159–167, February 2003.

[17] O.A. Ladyzhenskaya, *The Boundary Value Problems of Mathematical Physics*, Springer-Verlag, Berlin, 1985.

[18] K.S. St. Lawrence, T.Y. Lee, *An Adiabatic Approximation to the Tissue Homogeneity Model for Water Exchange in the Brain. I. Theoretical Derivation*, J. Cereb. Blood Flow Metab., Vol. 18, pp. 1365–1377, 1998.

[19] L. Østergaard, R.M. Weisskoff, D.A. Chesler, C. Glydensted, and B.R. Rosen, *High Resolution Measurement of Cerebral Blood Flow using Intravascular Tracer Bolus Passages. Part I: Mathematical Approach and Statistical Analysis*, Magn. Reson. Med., Vol. 36, pp. 715–725, 1996.

[20] A. Pazy, *Semigroups of Linear Operators and Applications to Partial Differential Equations*, Springer-Verlag, New York, 1983.

[21] E.M. Renkin, *Transport of Potassium-42 from Blood to Tissue in Isolated Mammalian Skeletal Muscle*, Am. J. Physiol., Vol 197, pp. 1205–1210, 1959.

[22] G. Strang, *The Discrete Cosine Transform*, SIAM Review, Vol. 41, No. 1, pp. 135–147, 1999.

[23] P.S. Tofts, *Modeling Tracer Kinetics in Dynamic Gd-DTPA MR Imaging*, J. Magn. Reson. Imaging, Vol 7, pp. 91–101, 1997.

[24] R.S. Varga, *Matrix Iterative Analysis*, Prentice-Hall, Englewood Cliffs, N. J., 1962.

[25] K.L. Zierler, *Theoretical Basis of Indicator-Dilution Methods for Measuring Flow and Volume*, Circulation Research, Vol. 10, pp. 393–407, March 1962.

[26] K.L. Zierler, *Theory of Use of Indicators to Measure Blood Flow and Extracellular Volume and Calculation of Transcapillary Movement of Tracers*, Circulation Research, Vol. 12, pp. 464–471, May 1962.